Helmholtz-Zentrum
Geesthacht
Zentrum für Material- und Küstenforschung

*Original*

Rao, K.P.; Bagheripoor, M.; Dieringa, H.; Hort, N.:

**High Temperature Deformation of Cast ZW11 Magnesium Alloy with Very Large Grain Size**

In: Key Engineering Materials, Advances in Engineering Plasticity and its Application XIII (2016) Trans Tech Publications

DOI: 10.4028/www.scientific.net/KEM.725.232

*Key Engineering Materials*
*ISSN: 1662-9795, Vol. 725, pp 232-237*
*doi:10.4028/www.scientific.net/KEM.725.232*
*© 2017 Trans Tech Publications, Switzerland*
*Submitted: 2016-05-15*
*Revised: 2016-07-10*
*Accepted: 2016-07-25*
*Online: 2016-12-15*

# High Temperature Deformation of Cast ZW11 Magnesium Alloy with Very Large Grain Size

K.P. Rao[1, a *], M. Bagheripoor[2,b], H. Dieringa[3,c] and N. Hort[3, d]

[1]Department of Mechanical and Biomedical Engineering, City University of Hong Kong, 83 Tat Chee Avenue, Kowloon, Hong Kong SAR, China

[2]Department of Mechanical and Materials Engineering, Western University, London, ON, Canada

[3]Helmholtz-Zentrum Geesthacht, Magnesium Innovation Centre, Max-Planck Str. 1, Geesthacht 21502, Germany

[a]mekprao@cityu.edu.hk, [b]mbagher6@uwo.ca, [c]hajo.dieringa@hzg.de, [d]norbert.hort@hzg.de

**Keywords:** Magnesium alloy, hot deformation, processing map, microstructure.

**Abstract.** Magnesium (Mg) alloys are considered for biomedical applications due to their matching bone density and biodegradable/abioabsorable nature. Mg-1% Zinc-1% Yttrium (ZW11) alloy was cast using a direct chill slow cooling process to obtain dense ingot with uniform composition. However, the resultant alloy developed a very coarse grained microstructure with a grain size in the range of 2,600 to 4,000 μm (2.6-4.0 mm). The hot working behavior of ZW11 alloy has been investigated using compression tests in the temperature and strain rate ranges of 340-540 $^{o}$C and 0.0003 – 10 $s^{-1}$ to evaluate the optimum processing parameters. A processing map has been developed on the basis of the flow stress data. The processing map reveals a window of workability in the temperature and strain rate ranges of 460-540 °C and 0.0003-10 $s^{-1}$ and regimes of flow instability. The microstructures of the deformed alloy provided support to the processing map.

## Introduction

The main considerations in the selection of Mg alloys for biodegradable implant applications are their corrosion rates, biocompatibility, and non-toxicity while they offer adequate strength and mechanical integrity. Zn has a good solid solubility and strengthens magnesium [1]. Zn helps to improve the corrosion resistance by combating the harmful effects of impurities and a maximum of about 3% is allowed for good corrosion resistance [2]. Attempts to improve strength, ductility and corrosion properties of Mg-Zn alloys are also being made with the addition of rare earth elements and yttrium addition is considered to be attractive [3]. When added to Mg-Zn alloy, Y improves its strength and increases the tensile elongation by modifying the texture [4]. The simultaneous presence of Y and Zn in Mg improves the creep strength [5]. The main aim of this research work is to determine the optimal conditions for thermomechanical processing of the cast Mg-1Zn-1Y (ZW11) alloy towards transforming it into wrought condition with good microstructure.

## Experimental Details

Mg-1Zn-1Y alloy was cast as a cylindrical billet using a modified permanent mold casting process, which resulted in a dense structure without blowholes and shrinkage porosity. Disks were cut from the casted cylinders and three samples were cut from the disk as shown in the schematic representation given in Fig. 1. Each sample was embedded in resin, ground, polished and etched for obtaining the microstructure. The same samples were then used for hardness testing. Hardness tests were performed using the HV5 test standard with an EMCOTEST M1C 010 machine. The measurements thus obtained are also shown in the figure, which indicate that the cast cylinder has extremely large grain structure in the range 2.6-4.0 mm while the hardness is fairly consistent across the section.

All rights reserved. No part of contents of this paper may be reproduced or transmitted in any form or by any means without the written permission of Trans Tech Publications, www.ttp.net. (#71145539, Helmoltz-Zentrum Geesthacht, Geesthacht, Germany-09/11/16,13:28:39)

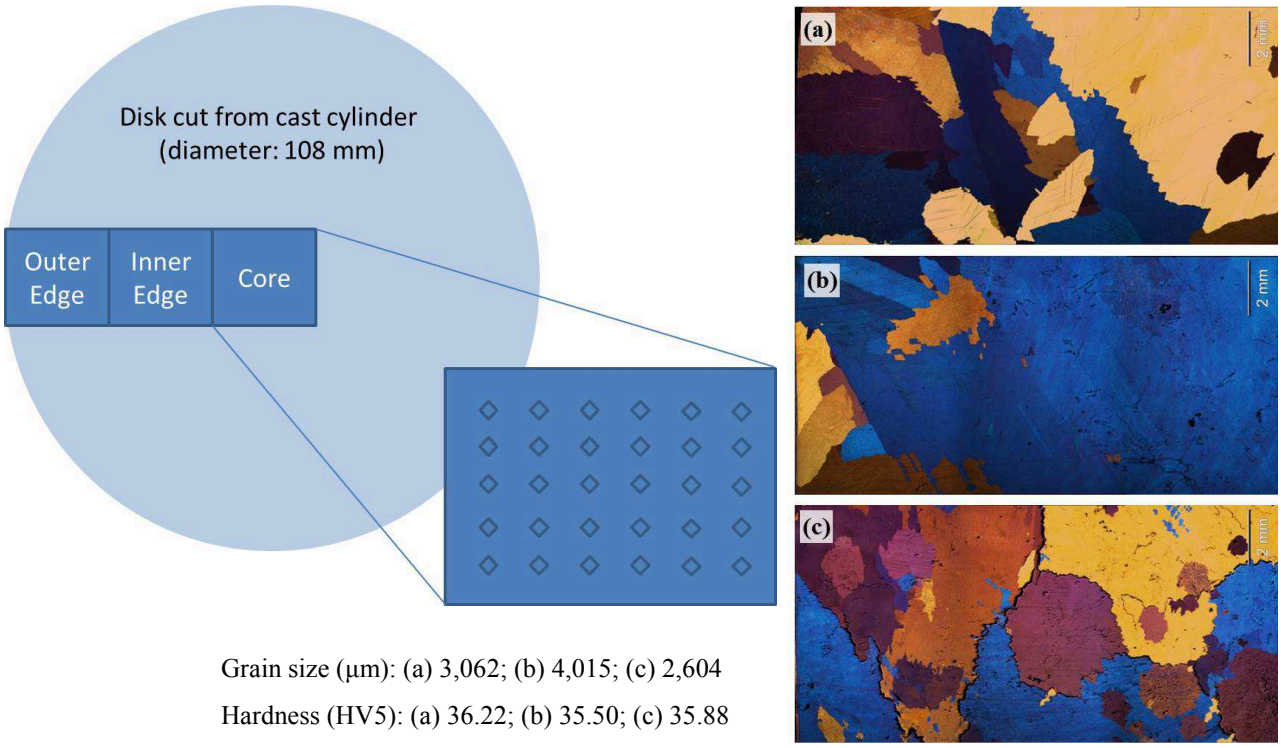


Fig. 1: Locations of the samples taken for microstructure and hardness testing along with the measurements – (a) outer edge, (b) intermediate section, and (c) central core of the billet.

Cylindrical specimens of 10 mm diameter and 15 mm height were machined from the as-cast billet for compression testing. A hole of 1 mm diameter and 5 mm depth was machined at mid-height to reach the center of the specimen for insertion of thermocouple to measure the specimen temperature during deformation. The compression test procedure was described in detail earlier [6]. The specimens were subjected to uniaxial compression in the temperature range of 340–540 °C and strain rate range of 0.0003–10 $s^{-1}$ using a 6x6 experimental matrix. An exponential decay in the actuator speed of the machine was used to achieve constant true strain rates during the compression tests. Graphite powder mixed with grease was used as the lubricant in all the experiments. The specimens were deformed up to a true strain of about 1 and quenched in water.

## Results and Discussion

**Deformed Specimens and Flow Curves.** The specimens deformed under the several combinations of temperature and strain rates are shown in Fig. 2. It can be seen that majority of the specimens have exhibited highly non-uniform flow indicating the possible difficulty in forming this alloy, and have been further studied through microstructural investigations.

The flow curves at 380 °C and 500 °C are shown in Fig. 3 for the six strain rates. The irregular variations of flow stress with strain and the absence of any systematic influence of strain rate in Fig. 3(a) reflect the non-uniform flow or fracture of the corresponding specimens shown in Fig. 2. For example, the flow curve corresponding to the strain rate of 0.001 $s^{-1}$ is lower than that of 0.0003 $s^{-1}$ and the former had fractured at a very low strain. In the case of those deformed at 500 °C, shown in Fig. 3(b), the curves exhibited the typical characteristics of dynamic recrystallization (DRX) in the form of flow-softening after a peak stress followed by steady-state stress at higher strain rates while they are of steady-state type at lower strain rates. The deformation conditions that exhibited flow curves similar to those in Fig. 3(b) are marked as 'Workability Domain' in Fig. 2, and the flow stress decreases with decrease in strain rate for a given temperature. Therefore, while the flow curves are obtained on a repeatable basis in the workability domain, they exhibited some random variations after the specimens fracture during deformation as in the case of tests at 380 °C (Fig. 3(a)).

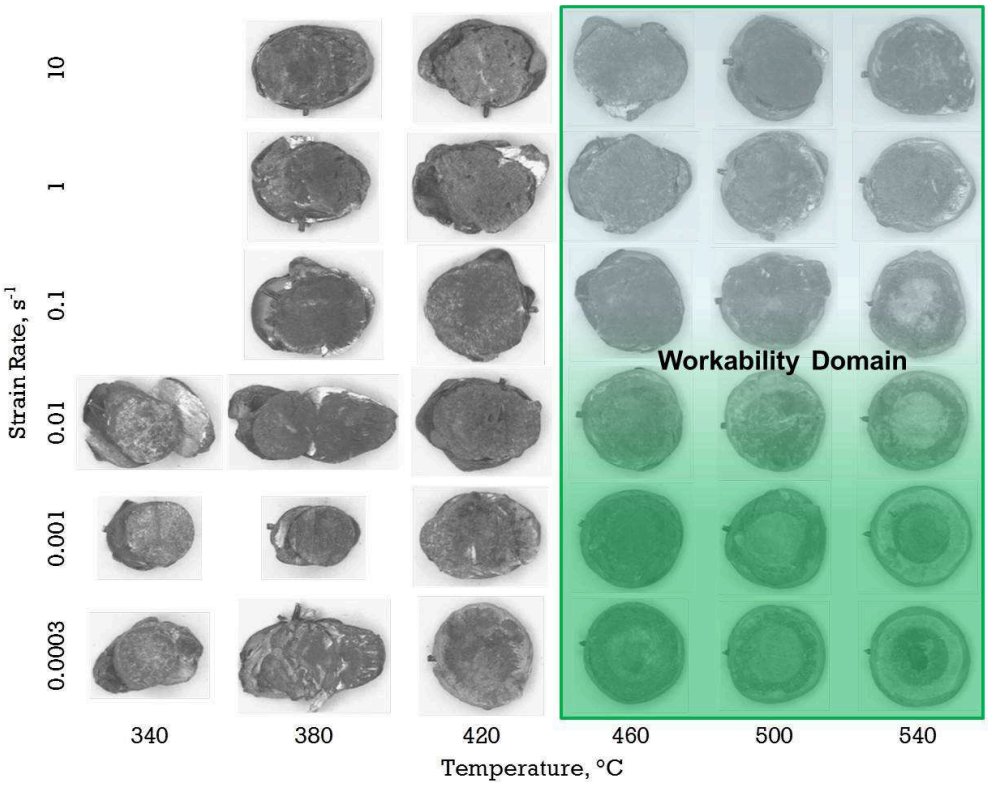


Fig. 2: Shapes of the specimens deformed at different temperatures and strain rates.

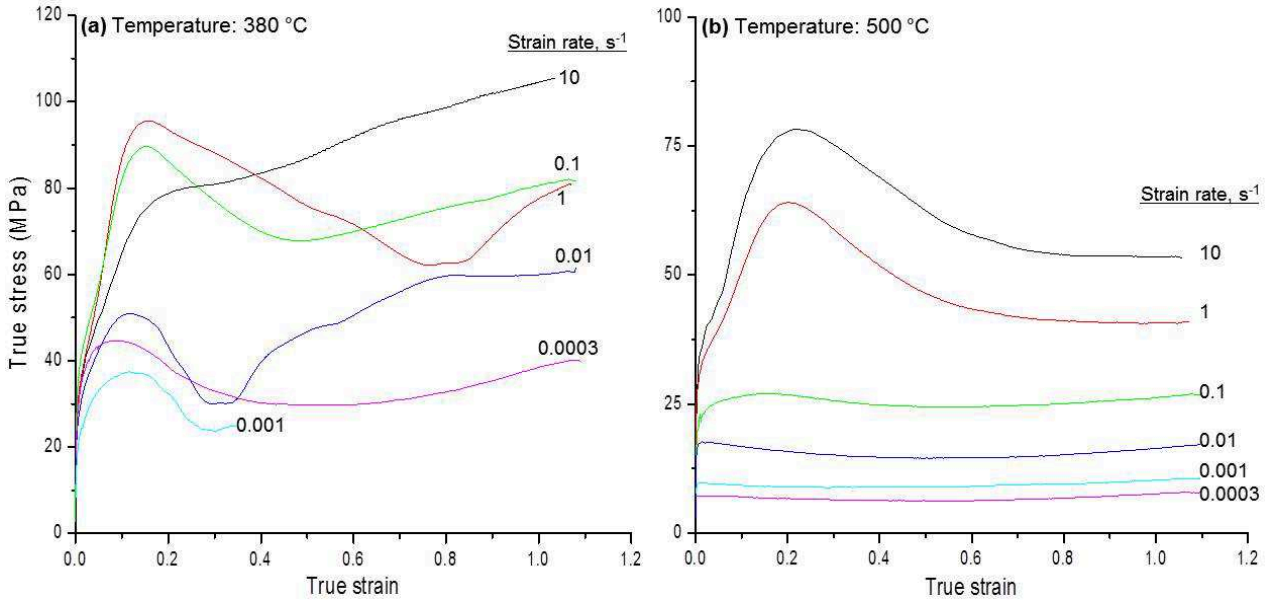


Fig. 3: Flow curves of ZW11 alloy at the temperatures of (a) 380 °C and (b) 500 °C for different strain rates.

**Processing Maps.** The principles and procedures for the development of processing map are described earlier [7]. Briefly, the processing map is a combination of power dissipation map and instability map, which are plotted as variation of power dissipation efficiency and instability parameter with temperature and strain rate, respectively. Basically the efficiency represents the proportion of applied power being utilized by the material towards metallurgical changes that occur during deformation. The map exhibits "domains" where the efficiency reaches a peak akin to mountains and separated by valleys representing the change-over from one domain to another. Each of the domains represents a metallurgical mechanism of power dissipation that may be identified on the basis of its characteristics and confirmed by microstructural examination of the deformed

specimens. The material may also undergo non-uniform deformation under certain conditions of processing and leads to flow instability. The microstructural manifestation of flow instabilities is typically adiabatic shear bands leading to internal fractures or flow localization that would result in non-uniform microstructures. By identifying suitable temperature-strain rate windows for hot working in which microstructurally "safe or good" processes like dynamic recrystallization (DRX) occur and by avoiding flow instability regimes, the workability may be optimized.

The flow stress values were corrected for the adiabatic temperature rise, which was measured during each compression test, to obtain the actual temperature. The corrected flow stress was computed by fitting smooth curves for flow stress data as a function of temperature at all relevant strain rates within the experimental points. The processing map was developed from the variation of corrected flow stress with temperature at different strains using the procedure described earlier [7]. The processing maps developed at the strain levels of 0.5 and 1.0, corresponding to the deformation beyond the peak stress and near steady state conditions, are shown in Fig. 4. The numbers associated with the contours represent efficiency of power dissipation in percent and the shaded areas represent flow instability regimes.

The processing map in Fig. 4 has revealed several regimes of flow instability. The map in Fig. 4(a) exhibits high level of power dissipation efficiency at high temperatures and low strain rates. With increase in strain, as can be seen from Fig. 4(b), the instability regime has shrunk and the high efficiency domain has expanded as the steady state conditions are reached. This can be considered as the processing map for material that can be used for large deformation situations such as those prevail in hot forming. The temperature and strain rate ranges for the workability domain are 460 – 540 $^{o}$C and 0.0003 – 10 $s^{-1}$ with a peak efficiency of about 46% occurring at 540 $^{o}$C/0.001 $s^{-1}$.

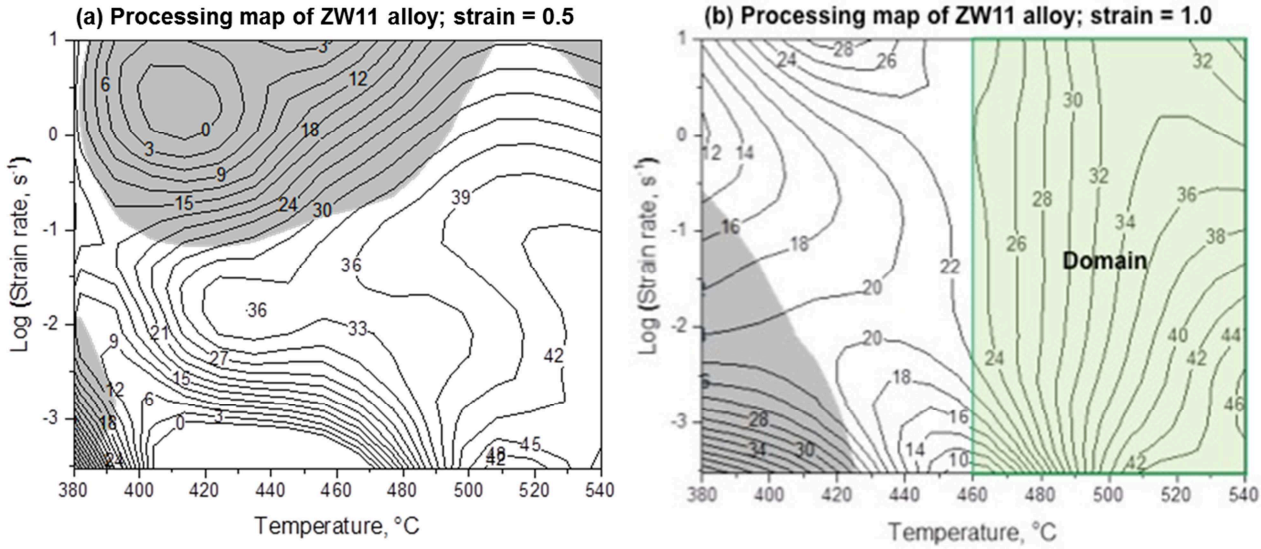


Fig. 4: Processing maps of ZW11 alloy at two different strain levels. The numbers for the contours are efficiencies of power dissipation and the shaded areas are flow instability regimes.

At lower temperatures, basal slip is highly favored due to its lower CRSS, although prismatic slip also occurs to some extent to satisfy the five slip system requirement in polycrystals for continuity of deformation across the grains. As the temperature is increased, the contribution from prismatic slip increases due to lowering of CRSS (critical resolves shear stress) and it dominates the deformation. The addition of Zn lowers the CRSS for prismatic slip [8] and further promotes its occurrence. The recovery mechanism that operates during deformation by either basal slip or prismatic slip is the thermal climb process since the mechanical recovery process, cross-slip, is restricted due to the non-availability of intersecting planes and lower stacking fault energy on the basal planes [9]. However, cross-slip is facilitated in 'Domain' due to higher temperatures, and the activation of a large number of pyramidal slip systems that lead to extensive material flow and dynamic recrystallization.

**Validation of Processing Maps.** The microstructures of the specimens deformed at 460 $^{o}$C at the six strain rates, i.e. start of workability domain, are shown in Fig. 5. The developed microstructures reveal complete recrystallization and the grain sizes are in the range of 30-60 μm, with finer grains corresponding to higher strain rates of deformation. The effect of temperature on the microstructure can be clearly understood from the micrographs of the specimens deformed at a strain rate of 1 $s^{-1}$, as given in Fig. 6. It can be seen that the specimen deformed at 380 °C has shown extensive localization of material flow and shear bands along with some finely recrystallized grains at the severely deformed areas. With an increase in the deformation temperature to 420 °C, while the microstructure has indicated significant level of recrystallization, the existence of localized material flow is also evident. However, the microstructures of the specimens deformed at 460 °C and higher temperatures have exhibited completely recrystallized and uniform grains. The grain size increased significantly from about 30 μm at 460 °C to 120 μm at 540 °C in the workability domain.

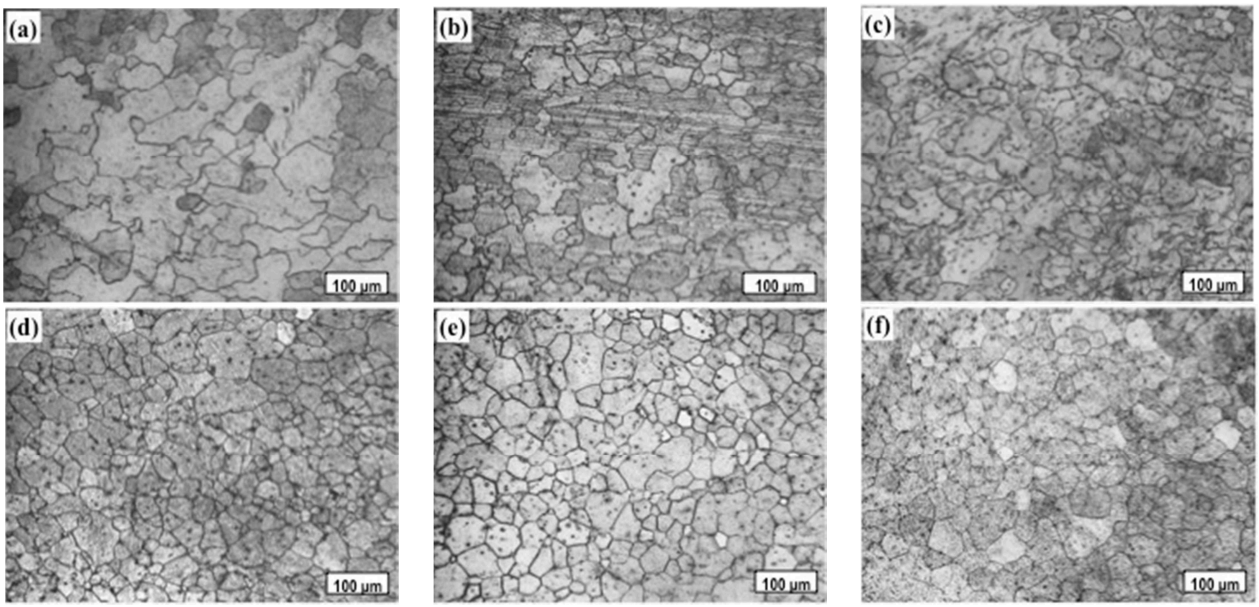


Fig. 5: Microstructures of ZW11 alloy deformed at 460 °C and six strain rates of (a) 0.0003 $s^{-1}$, (b) 0.001 $s^{-1}$, (c) 0.01 $s^{-1}$, (d) 0.1 $s^{-1}$, (e) 1 $s^{-1}$, and (f) 10 $s^{-1}$.

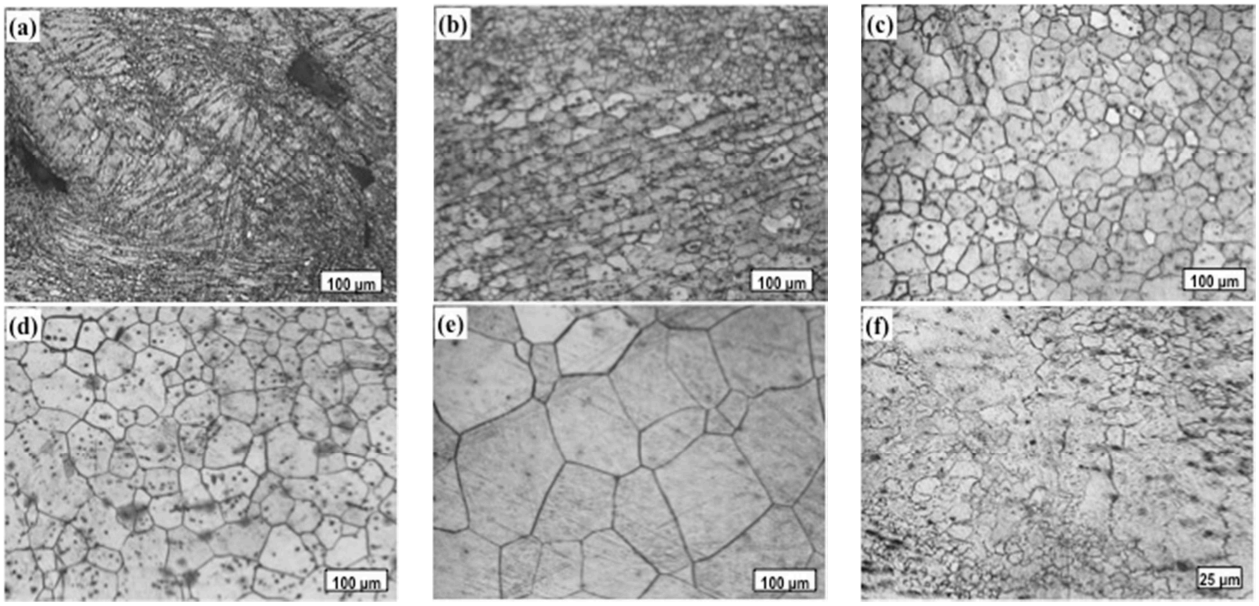


Fig. 6: Microstructures of ZW11 alloy deformed under a strain rate of 1 $s^{-1}$ at (a) 380 °C, (b) 420 °C, (c) 460 °C, (d) 500 °C, and (e) 540 °C. Microstructure of the deformed alloy at 380 °C under a strain rate of 0.0003 $s^{-1}$ is shown in (f) at a higher magnification.

The processing map in Fig. 4(b) has revealed regime of flow instability at low temperatures and low strain rates. However, the efficiency of deformation is also significant. The microstructure of specimens deformed at 380 °C under the strain rate of 0.0003 $s^{-1}$, given in Fig. 6(f), indicates that there is partial recrystallization along the localized flow bands.

## Summary

Mg-1Zn-1Y (ZW11) alloy has been tested in compression with a view to evaluate its high temperature deformation characteristics. At lower temperatures and higher strain rates, the alloy exhibits flow instability in the form of highly localized material flow. The processing map developed exhibited one high efficiency domain in the ranges 460-540 $^{o}$C and 0.0003–10 $s^{-1}$. Dynamic recrystallization readily occurs in the workability domain, and pyramidal slip is dominant that assists large-scale deformation. The recovery mechanism leading to dynamic recrystallization is climb of edge dislocations at lower strain rates and cross-slip at higher strain rates. Although the resultant grain size is large at higher temperature, it ensures easy conversion of the cast alloy into wrought condition. High productivity can be achieved by selecting secondary or finish forming at the lower end of temperature and the higher end of strain rate within the workability domain to obtain fine grain size and high strength.

## Acknowledgement

Support from the Research Grants Council of Hong Kong through project no. G_HK006/12 as well as DAAD through project “Magnesiumlegierungen für biodegradable Anwendungen”, project-ID 56203444 is acknowledged. The authors thank Dr. K. Suresh, Assistant Professor, Department of Physics, Bharathiar University, Coimbatore, India, for his help with the microstructural work.

## References

[1] C.J. Boehlert, K. Knittel, The microstructure, tensile properties, and creep behavior of Mg-Zn alloys containing 0 - 4.4 wt% Zn, Materials Sci. and Eng. A417 (2006) 315-321.

[2] G. Song, A. Atrens, Corrosion mechanisms of magnesium alloys, Advanced Engineering Materials. 1 (1999) 11-33.

[3] B.Q. Shi, R.S. Chen, W. Ke, Effects of yttrium and zinc on the texture, microstructure and tensile properties of hot-rolled magnesium plates, Mater. Sci. and Eng. A560 (2013) 62-70.

[4] S.A. Farzadfar, M. Sanjari, I.H. Jung, E. Essadiqui, S. Yue, Role of yttrium in the microstructure and texture evolution of Magnesium, Mater. Sci. and Eng. A528 (2011) 6742-6753.

[5] M. Suzuki, T. Kimura, J. Koike, K. Maruyama, Effects of Zn on creep strength and deformation substructures in Mg-Y alloys, Mater. Sci. and Eng. A387-389 (2004) 706-609.

[6] Y.V.R.K. Prasad, K.P. Rao, Processing maps and rate controlling mechanisms of hot deformation of electrolytic tough pitch copper in the temperature range 300 – 950 $^{o}$C, Mater. Sci. and Eng. A391 (2005) 141-150.

[7] Y.V.R.K. Prasad, K.P. Rao, S. Sasidhara, Hot Working Guide: A Compendium of Processing Maps, Second edition, ASM International, 2015.

[8] A.H. Blake, C.H. Caceres, Solid solution effects on the tensile behaviour of concentrated Mg-Zn alloys, in: N.R. Neelameggham, H.I. Kaplan and B.R. Powell (Eds.), Magnesium Technology 2005, TMS, Warrendale, 2005, pp. 263-267.

[9] D.H. Sastry, Y.V.R.K. Prasad, K.I. Vasu, On the stacking fault energies of some close-packed hexagonal metals, Scripta Metall. 3 (1969) 927-930.